Applied Catalysis B: Environmental 147 (2014) 101–110

Contents lists available at ScienceDirect

Applied Catalysis B: Environmental

journal homepage: www.elsevier.com/locate/apcatb

CO_2 hydrogenation into CH_4 on NiHNaUSY zeolites

I. Graça, L.V. González, M.C. Bacariza, A. Fernandes, C. Henriques, J.M. Lopes, M.F. Ribeiro*

IBB, Institute for Biotechnology and Bioengineering, Centre for Biological and Chemical Engineering, Instituto Superior Técnico, UTL, Av. Rovisco Pais, 1049-001 Lisboa, Portugal

ARTICLE INFO

Article history:
Received 9 April 2013
Received in revised form 1 August 2013
Accepted 7 August 2013
Available online 20 August 2013

Keywords:
Carbon dioxide
Methanation
Zeolites
Nickel
Cerium

ABSTRACT

CO_2 hydrogenation into methane was carried out over catalysts containing nickel and cerium species supported on a HNaUSY zeolite, using an H_2/CO_2 ratio of 4 and temperatures ranging from 250 to 450 °C. Interesting CO_2 conversions and CH_4 selectivities were achieved for Ni-zeolite catalysts prepared by impregnation. Conversion increased with the Ni content from 2 to 14%, due to the higher amount of Ni^0 species after reduction. A further enhancement of the catalysts performances was noticed when doping the Ni-zeolites catalysts with 3–15% of Ce. Actually, the presence of CeO_2 after reduction might promote CO_2 activation into CO, the final catalyst properties being due to the synergetic effect between the metal active sites and the promoter. Furthermore, almost no deactivation due to sintering was observed after 10 h of reaction at 400 °C. Comparing these results with those reported in literature it is possible to conclude that zeolites have great potential to be used as catalyst supports for the CO_2 methanation reaction. In fact, taking the commercially available and widely used HNaUSY zeolite, it was possible to reach conversions and selectivities similar to those previously found in the literature for the best CO_2 methanation catalysts that use potentially more expensive bulk cerium oxide supports, even without performing any optimization of the zeolite support.

1. Introduction

Increasing emissions of carbon dioxide arising from the widespread production of energy from fossil fuels is a critical matter regarding greenhouse gases effect and, thus, global warming. Many efforts have been done to develop low-carbon energy alternatives and renewable energy sources based processes to reduce CO_2 emissions. However, the consumption of fossil fuels is still expected to growth in the coming years due to the increasing worldwide demand for energy, mainly caused by the emerging economies. In fact, CO_2 emissions should exceed 40 Gt/year by 2030 [1]. On the other hand, the European Commission has defined tight targets concerning the reduction of the CO_2 emissions (60–80% by 2050 [2]).

Important amounts of CO_2 are emitted from electric power plants consuming coal or natural gas and industrial plants, such as cement [3], which usually represent a negative value for the industries when considering the carbon taxes. Therefore, instead of a waste, it would be quite interesting to use CO_2 as source of carbon. Beyond CO_2 sequestration and geological storage that are expensive and energetically not sustainable options [4], the possibility of producing chemicals and fuels from CO_2 represents a quite attractive alternative. Nowadays, CO_2 is already used as raw-material in a few chemical processes: synthesis of urea and its derivatives, production of organic carbonates and salicylic acid [5]. However, taking into account the huge amounts of CO_2 emissions, the production of fuels should be considered as the most effective option for their reduction, due to the higher consumption rates in the fuels sector [5].

The hydrogenation of CO_2 into oxygenates and/or hydrocarbons (methane, methanol or dimethyl ether) have been the most investigated reactions to obtain fuels [3,5–8]. Among several hydrogenation reactions, methanation of carbon dioxide following the Sabatier reaction ($CO_2 + 4H_2 \leftrightarrow CH_4 + 2H_2O$) is the most advantageous one regarding thermodynamics [9]. In addition, as methane is the main component of natural gas (NG), it can be safely transported using the existing NG infrastructures [10].

Extensive studies have been carried out on metal-based catalytic systems for the CO_2 methanation reaction, namely group VIIIB metals (Fe, Ru, Co, Rh, Ir, Ni, Pd, Pt) supported on several oxides (e.g., SiO_2, TiO_2, Al_2O_3, ZrO_2, CeO_2 and Ce–Zr mixed oxides) [11]. So far, Ni, Ru and Rh have revealed as the most effective metals for this reaction [11–15], Ru and Rh having been reported as the most selective towards methane [12,15]. However, nickel covers the larger part of published works [11], since it is a cheaper metal, and so more interesting from the commercial standpoint. The main reported problem of Ni-based catalysts seems to be the deactivation at low temperature due to the interaction of the metal particles with CO and the formation of mobile nickel carbonyls that lead to the metal sintering [16,17]. A partial solution for this question

* Corresponding author. Tel.: +351 21 841 7872; fax: +351 21 841 9198.
E-mail address: filipa.ribeiro@ist.utl.pt (M.F. Ribeiro).

0926-3373/$ – see front matter © 2013 Elsevier B.V. All rights reserved.
http://dx.doi.org/10.1016/j.apcatb.2013.08.010

could be the promotion of Ni catalysts with noble metals (e.g. Ru and Rh), as noble metals are known to prevent the sintering effect by increasing the dispersion of Ni particles [18].

Another important issue concerning the activity, selectivity and stability of catalysts is the nature of the support. In fact, the different interactions that can be established between the metal and the support shall influence the catalytic properties of the active metal sites [11]. Cerium oxides and Ce–Zr mixed oxides based catalysts have presented the most interesting properties for the methanation reaction [18–23]. Recently, Tada et al. [21] studied the effect of different supports, CeO_2, α-Al_2O_3, TiO_2 and MgO, containing the same amount of metal (10% Ni), on the CO_2 hydrogenation into methane. Ni/CeO_2 catalyst showed the highest CO_2 conversions at lower temperatures and CH_4 selectivities very close to 100%. The better performances of CeO_2 were attributed to its higher ability to adsorb CO_2 molecules, to reduce them into CO and to convert CO into CH_4. A similar behaviour had already been observed by Trovarelli et al. [22,23], who compared the catalytic activity of several Rh-based catalysts using different types of supports: CeO_2, SiO_2, Ta_2O_2 and Nb_2O_5. The CO_2 methanation reaction using Ni supported on Ce–Zr mixed oxides catalysts was for the first time investigated by Ocampo et al. [18,19]. They found that these catalysts exhibited excellent levels of activity, selectivity and stability for CO_2 methanation. Furthermore, CeO_2 has been as well successfully used as catalysts promoter. In fact, whatever the support (Al_2O_3 or SiO_2) and the metal used (Ni or Ru), samples promoted with CeO_2, mainly at low CeO_2 loadings, demonstrated an improved activity for the CO_2 hydrogenation into methane [23–25]. According to the literature [18–26], the astonishing performances observed for the catalysts containing CeO_2, as support or promoter, are ascribed to (i) the CeO_2 ability to create oxygen bulk vacancies that promote the CO_2 reduction into CO and/or surface carbonaceous species, which rapidly hydrogenate to CH_4, (ii) the effectiveness of its Ce^{3+}/Ce^{4+} couple that is also suggested to be involved in the CO_2 activation and (iii) the capacity to highly disperse metals.

Despite the encouraging results found for the CO methanation over zeolite supports, given that identical initial turnover numbers were found for Ru/Y and Ru/Al_2O_3 catalysts [27], as well as an increase of the catalysts activity by supporting Pd on zeolites instead of SiO_2, in the order HY > HZSM-5 > NaZSM-5 $\gg$ NaY > SiO_2 [28], the use of zeolites for CO_2 methanation has been scarce [29–31]. CO_2 hydrogenation into CH_4 was investigated over Ru/HZSM-5 and Ru/SiO_2 catalysts, being the former catalyst more selective to CH_4 [29]. Authors sustain that the quite higher methane selectivity observed on Ru/HZSM-5 was due to the stronger metal-support interaction, as well as to the higher amount of CO_2 molecules interacting with the zeolite, resulting from the CO_2 interaction with the OH-groups of the zeolite. It was noticed that this interaction leads to the loss of the CO_2 molecular symmetry and, consequently, to the dissociation of CO_2 into CO. Eckle et al. [30], based on in-situ IR spectroscopy measurements, also proposed that the CO_2 methanation reactions over Ru/zeolite catalysts proceeds via dissociative adsorption of CO_2 to form CO_{ad} and O_{ad}, which subsequently reacts to CH_4 and H_2O. Furthermore, an enhanced CH_4 formation was observed for Y zeolite samples with higher mesoporosity, as a consequence of improved kinetics [31].

Hence, the main goal of this work was to evaluate the possibility of preparing catalysts based on Ni and Ce species supported on an ultra-stable partially exchanged HNaUSY zeolite (commercially available and widely used zeolite) that could present interesting properties towards the selective CO_2 hydrogenation into methane, when compared to the best cases previously studied and published reporting the use of potentially more expensive rare earth oxides bulk supports. Several catalysts samples, containing different Ni amounts, were prepared by ion-exchange and impregnation, and deeply characterized by many relevant techniques, so that some insights concerning the understanding of the catalytic promotion could be obtained. The impact of doping these catalysts with Ce was also investigated. Moreover, the stability of the catalysts was evaluated, by submitting the catalysts to 10 h of reaction at 400 °C.

2. Experimental

2.1. Catalysts preparation

The ultra-stable Y (USY) zeolite was supplied by Grace Davidson. Its physicochemical properties are given in Table 1. The introduction of Ni on the zeolite support was carried out by ion-exchange (2 wt.%) and incipient wetness impregnation (2–14 wt.%), using nickel nitrate hexahydrate ($Ni(NO_3)_2{\cdot}6H_2O$, Merck, >99%) in both cases as metal precursor. The catalysts were referred as x%$NiUSY_{Ex}$ and x%$NiUSY_{Imp}$ (x = Ni content), respectively. Concerning ion-exchange, the initial zeolite was dispersed in a 0.012 M aqueous solution of $Ni(NO_3)_2{\cdot}6H_2O$ and the suspension was stirred at 80 °C for 24 h, under reflux, after which it was filtered and washed with deionised water. For the incipient wetness impregnation, an aqueous solution of $Ni(NO_3)_2{\cdot}6H_2O$ with a volume of water close to that of the zeolite pores was added drop by drop to the zeolite. The suspension was kept under stirring while adding the precursor solution. After Ni ion-exchange and impregnation, the catalysts were dried overnight at 80 °C then calcined at 500 °C under dry air flow (60 mL min^{-1} g^{-1}). A mechanical mixture of 10 wt.% of NiO and USY zeolite was also prepared by simply mixing a commercial NiO (Aldrich, 99%) with the zeolite.

Doping with Ce (3–15 wt.%) was performed through incipient wetness impregnation of Ni catalysts. Only the Ni catalysts prepared by incipient wetness impregnation were doped with Ce. Cerium acetate sesquihydrate ($Ce(C_2OOH_3)_3{\cdot}1.5H_2O$, Alfa Aesar, 99.9%) was chosen as metal salt. After Ce impregnation, the catalysts were dried overnight at 80 °C and then calcined at the same conditions previously described. The Ce–Ni catalysts were called x%Niy%$CeUSY_{Imp}$, in which x is the amount of Ni and y the Ce content, respectively. Moreover, a sample only containing Ce (7 wt.%), 7%$CeUSY_{Imp}$, was prepared by incipient wetness impregnation, using the same procedure.

2.2. Catalysts characterization

Prepared catalysts, after calcination and before in-situ reduction, were characterized by elemental analysis, nitrogen adsorption, hydrogen temperature programmed reduction (H_2-TPR), UV–vis diffuse reflectance spectroscopy (DRS) and X-ray diffraction (XRD).

Catalysts chemical composition was determined by elemental analysis through inductively coupled plasma (ICP) and atomic absorption (AA).

Nitrogen adsorption measurements were carried out at −196 °C on a Micrometrics ASAP 2010 apparatus. Before adsorption, zeolite samples were degassed under vacuum at 90 °C for 1 h and then at 350 °C for 4 h. The total pore volume (V_{total}) was calculated from the adsorbed volume of nitrogen for a relative pressure P/P_0 of 0.97, whereas the micropore volume (V_{micro}) and the external surface area (S_{ext}) were determined using the t-plot method [33,34]. The mesopore volume (V_{meso}) was given by the difference $V_{total} - V_{micro}$.

H_2-TPR tests were accomplished in a Micromeritics AutoChem II equipment. Catalysts were pre-treated at 250 °C under argon flow and then cooled down to the room temperature. Reduction of the catalysts was carried out by flowing a H_2 (5 vol.%)/argon mixture, rising the temperature from the room temperature to 900 °C. The hydrogen consumed was monitored by a TCD detector.

Table 1
Physicochemical properties of the commercial USY zeolite.

Unit cell formula	Si/Al[a]	Si/Al_{IV} [b]	V_{micro} ($cm^3\ g^{-1}$)	V_{meso} ($cm^3\ g^{-1}$)	S_{ext} ($m^2\ g^{-1}$)
$Na_{16}H_{21}Al_{37}Si_{142}O_{384}$, 13EFAL	2.8	3.8	0.286	0.041	17

Note. V_{micro}: micropore volume; V_{meso}: mesopore volume; S_{ext}: external surface area.
[a] Global Si/Al ratio determined from elemental analysis.
[b] Framework Si/Al ratio calculated from the unit cell parameter (a_0 = 2.535 nm), using the Breck–Flanigen equation [32].

DRS spectra in the UV–vis region were obtained in a Varian Cary 5000 UV–Vis–NIR spectrophotometer, equipped with a diffuse reflectance accessory (integration sphere, DRA-2500), in the 200–800 nm range. Catalysts spectra were obtained using the USY zeolite as reference. The reflectance spectra were converted into the Schuster–Kubelka–Munk (SKM) function, $F(R)$, and presented versus wavelength. The SKM function, $F(R)$, was calculated from the reflectance, at each wavelength, using the expression: $F(R) = (1-R)^2/2R$, where R is the ratio of the intensity of the light reflected by the sample to the one reflected by a standard.

The XRD powder patterns were obtained in a Bruker AXS AdvanceD8 diffractometer, using Cu Kα radiation and operating at 40 kV and 40 mA. The scanning range was set from 5° to 80° (2θ), with a step size of 0.03°/2 s.

Samples after reduction were analyzed by transmission electron microscopy (TEM) using a Hitachi 8100 with ThermoNoran light elements and EDS detector, as well as by XRD using the procedure previously described.

2.3. Catalytic tests

Catalytic tests were carried out in a flow tubular reactor in Pyrex, under atmospheric pressure. Before the reaction, catalysts were pre-reduced in-situ at 470 °C during 1 h, under a 80%H_2/N_2 stream, with a total gas flow of 250 $cm^3\ min^{-1}$. For the reaction, a mixture of hydrogen, carbon dioxide and nitrogen was fed into the reactor, at a molar ratio of H_2:CO_2:N_2 = 36:9:10 and a total flow of 250 $cm^3\ min^{-1}$. Hydrogen, carbon dioxide and nitrogen flows were controlled by calibrated Brooks mass flow metres. All gases were supplied by Air Liquid, with purities ≥99.9990%. Reaction was performed at temperatures ranging from 250 to 450 °C, at gas hourly space velocities (GHSV) of 43,000 h^{-1} and 15,000 h^{-1}. Products were analyzed using a CO_x Siemens Ultramat 23 infrared detector, to measure the concentrations of CO and CO_2 present in the reactor effluent, and a 5890 HP Series II Gas Chromatograph (GC), equipped with a Poraplot Q capillary column (25 m, helium as carrier gas) and a flame ionization detector (FID), to determine the amount of methane produced. At each temperature, after the stabilization of the catalytic system, three measures of CO, CO_2 and CH_4 were taken and an average value was calculated. In order to analyze the stability of the catalysts, deactivation tests were accomplished at a constant temperature of 400 °C and GHSV = 43,000 h^{-1}, during 10 h, using the reaction conditions described above.

Furthermore, thermodynamic equilibrium conversions and selectivities for this catalytic system were determined using the Aspen Plus® software, with a Gibbs reactor, in which the equilibrium values are calculated through the minimization of the Gibbs free energy. The components chosen were CO_2, H_2, CH_4, H_2O, N_2 and CO and the operating conditions used in the programme were identical to those of the catalytic tests.

3. Results and discussion

3.1. Catalysts characterization

3.1.1. Ni–Y catalysts

Fig. 1 shows the UV–vis spectra obtained for all the catalysts containing Ni. The UV–vis spectra of the catalysts prepared by ion-exchange and impregnation with 2% of Ni are quite similar, presenting coincident bands at around 410, 650 and 740 nm, which reveal the presence of octahedral Ni^{2+} species. According to the literature [35–37], the 410 and 650 nm bands have been assigned to the d-d spin-allowed electronic transitions of octahedrally coordinated Ni^{2+} species, while the band at 740 nm has been attributed to d-d spin-forbidden transition in octahedral Ni^{2+}. For the 2% Ni sample prepared by impregnation, another two less intense bands can be observed: a band at around 300 nm and a shoulder at 450 nm, which indicate the presence of NiO species [38]. This can also be confirmed by the analysis of the UV–vis spectrum of NiO (Fig. 1b), which exhibits four main bands at about 290, 388, 430 and 725 nm, in agreement with the literature [38]. With the increase of the Ni content (5–14%) on the impregnated zeolites, the bands corresponding to the octahedral Ni^{2+} species disappear, remaining those related to the NiO species: 300, 390, 429 and 725 nm, their intensity increasing with the increase of Ni content.

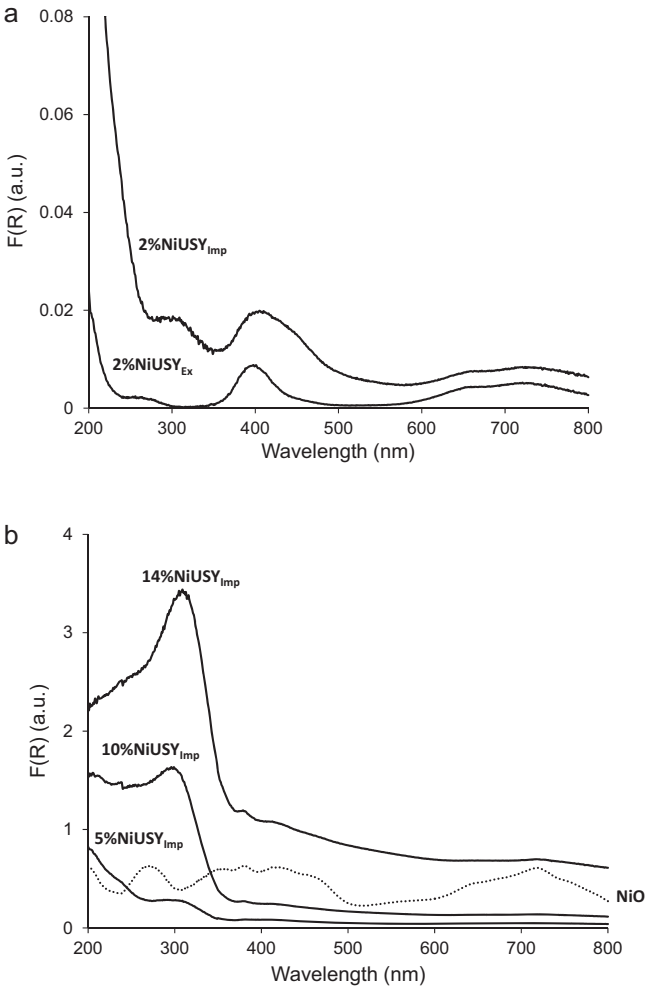

Fig. 1. DRS UV–vis spectra obtained (a) for the catalysts prepared by ion-exchange and impregnation with 2% of Ni, and (b) for the catalysts prepared by impregnation containing 5–14% of Ni and NiO.

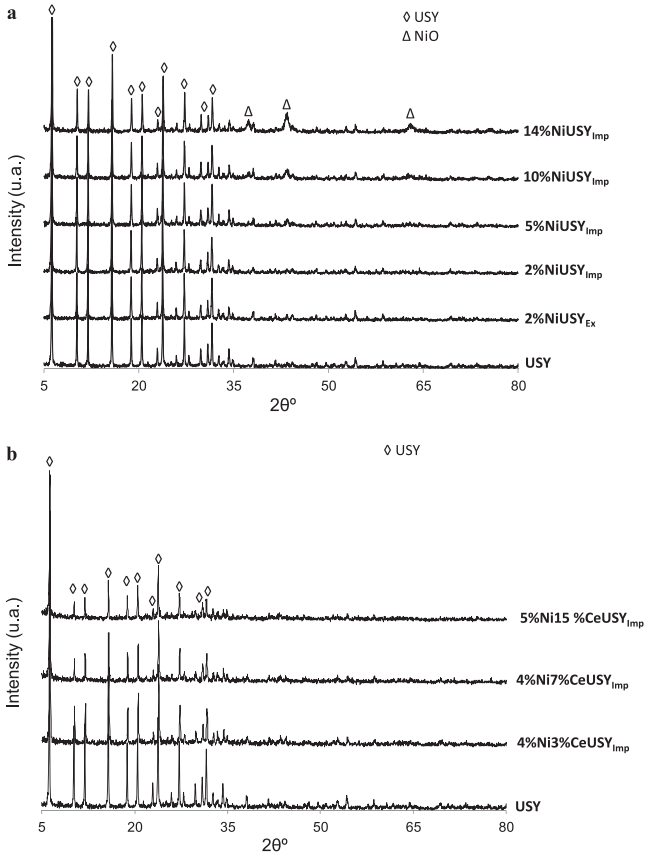

Fig. 2. X-ray diffractograms for the catalysts (a) containing Ni, and (b) containing Ni and Ce.

The presence of NiO on the highly Ni impregnated zeolites was confirmed by XRD (Fig. 2a), for which the patterns, besides the XRD characteristic reflections of the crystalline FAU structure, exhibit reflections at about 37°, 43° and 63° attributed to the presence of NiO [19], whose intensity also increases with the amount of Ni.

H_2-TPR profiles of Ni zeolites are presented in Fig. 3. For the 2% Ni sample obtained by ion-exchange (Fig. 3a), a single reduction band appears at around 850 °C, which might be associated with the reduction of Ni^{2+} located in hexagonal prisms [39]. Usually, most of the Ni^{2+}-exchanged ions on Ni-faujasite structures are positioned at the centre of hexagonal prisms, in which Ni^{2+} ions attain a near-perfect octahedral coordination with the six framework oxygen atoms, being much more stable than tetrahedrally coordinated Ni^{2+} ions at the supercages and sodalite cages [39,40]. In fact, only octahedral Ni species were observed for this sample by UV–vis spectroscopy. On the other hand, the impregnated Ni zeolites present four main reduction bands (Fig. 3a and b). The band at the lowest temperature, with a maximum around 350–400 °C, can be ascribed to the reduction of NiO particles located on the outer surface of the zeolite, which are more easily reduced [41–44]. This can also be confirmed by the TPR profile obtained for the mechanical mixture of USY and NiO, in which the reduction band for the bulk NiO appears at about 420 °C (Fig. 3b). The other reduction processes show maxima at around 500, 600 and 800 °C, which could be related to the reduction of Ni^{2+} species located on the supercages, sodalite cages and hexagonal prisms of the zeolites, respectively [42–44]. Furthermore, it is possible to note that, for the sample containing 2% of Ni, the main reduction band is that corresponding to the reduction of Ni^{2+} located on the hexagonal prisms with octahedral coordination, whereas, for the catalysts containing 5–14% of Ni, the dominant reduction process is

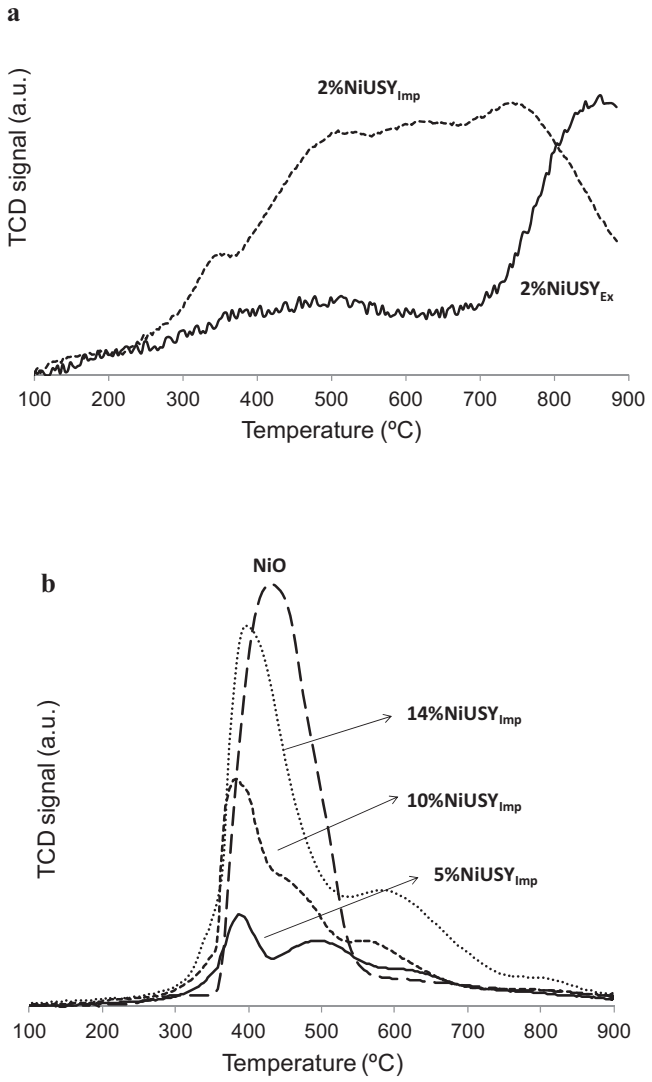

Fig. 3. H_2-TPR profiles obtained (a) for the catalysts prepared by ion-exchange and impregnation with 2% of Ni and (b) for the catalysts prepared by impregnation containing 5–14% of Ni and NiO.

Table 2
Microporous volume and external surface area for Ni catalysts.

Sample	V_{micro} ($cm^3\ g^{-1}$)	S_{ext} ($m^2\ g^{-1}$)
USY	0.286	17
2%NiUSY$_{Ex}$	0.275	21
2%NiUSY$_{Imp}$	0.253	11
5%NiUSY$_{Imp}$	0.280	13
10%NiUSY$_{Imp}$	0.210	14
14%NiUSY$_{Imp}$	0.222	14

the one attributed to the outer surface NiO species. The amount of NiO on the zeolites increases with the Ni amount. All these results perfectly agree with the UV–vis spectroscopy data obtained.

The values of microporous volume and external surface area of the different Ni catalysts are given in Table 2. In general, it can be observed that the addition of Ni leads to a decrease of the microporous volume. However, this reduction is not extremely pronounced, even for catalysts presenting high metal contents, meaning that, for all samples, the active sites of the catalysts are accessible to the reactant molecules. There is also a decrease of the external surface area with the Ni addition, which could suggest a deposition of the Ni species on the external surface of the zeolite,

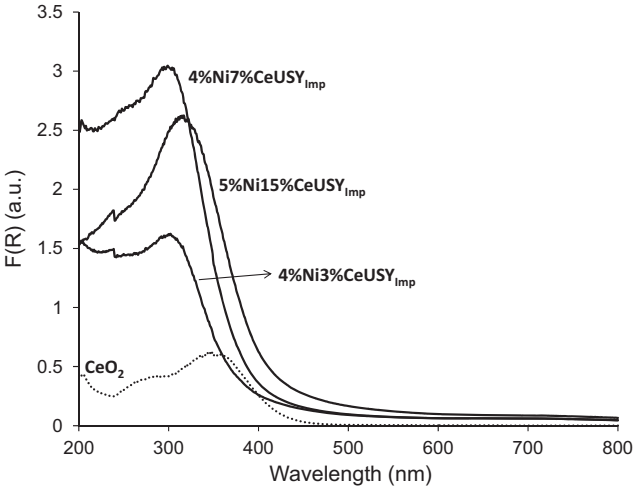

Fig. 4. DRS UV–vis spectra obtained for the catalysts presenting both Ni and Ce.

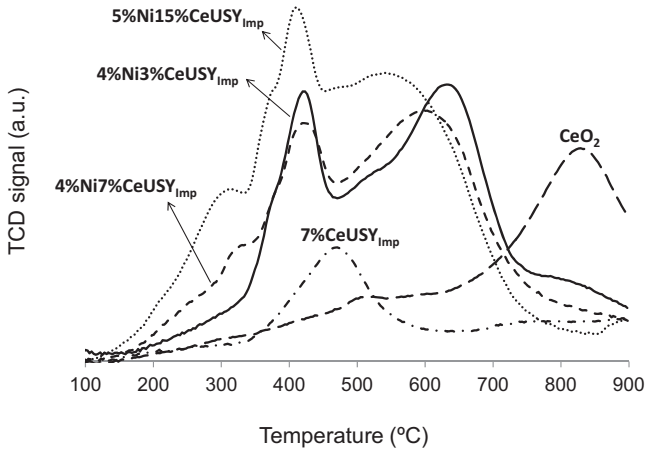

Fig. 5. H_2-TPR profiles of Ni–Ce catalysts.

explaining possibly in part the reduction of the microporous volume. This might as well confirm the location of NiO species on the external surface of the zeolite.

3.1.2. Ni–Ce–Y catalysts

The UV–vis spectra of the catalysts presenting both Ni and Ce are depicted in Fig. 4. First, by comparing Fig. 1b and 4, it is possible to observe that Ni and doped Ce catalysts present a large coincident UV–vis band at ~300 nm. In fact, there is an increase of the intensity of this band by adding Ce to the Ni catalysts. This massif noticed for the Ni–Ce zeolites are composed by two main bands, one at 260 nm and other at about 310 nm, which are attributed to 4f-5d interconfiguration transitions of Ce^{3+} and to the presence of CeO_2, respectively [45]. The intensity of the band assigned to CeO_2 is higher, meaning that these Ce species are more abundant on the catalysts. The presence of CeO_2 on the catalyst can be confirmed by analyzing the UV–vis spectrum of the bulk CeO_2, in which a main band appears at around 360 nm, while a smaller one is observed at 290 nm. It is claimed in the literature that CeO_2 bands are usually shifted to lower wavelengths when finely dispersed on a support [46,47]. These finer CeO_2 crystallites normally escape to XRD detection, as can be noticed in Fig. 2b. No peaks related to the fluorite structure of CeO_2 ($2\theta = 28.6^\circ$, 33.3° and 47.5°) are observed [48]. Moreover, the XRD patterns of Ce doped zeolites reveals that the increase of Ce content leads to a decrease of the relative intensity of all the peaks. This effect was referred in the literature [48,49] as being due to the high cerium absorption coefficient of X-ray radiation.

The H_2-TPR profiles of Ni–Ce catalysts are displayed in Fig. 5. For these samples, two major reduction peaks were found, one at around 400 °C corresponding to NiO and another at higher temperature (~600 °C) related to ceria reduction. Analyzing Fig. 5, it can be observed that there was no change in the NiO reduction temperature due to Ce addition. On the other hand, the CeO_2 reduction seems to be affected by the presence of Ni, so that an interaction between Ni and Ce could exist. Actually, when only Ce is impregnated on the support (7%CeUSY$_{Imp}$) as CeO_2 (confirmed by UV–vis spectroscopy, spectrum not shown), a single reduction process can be found at about 460 °C. According to the literature [50], the existence of reduction peaks at temperatures below 600 °C for the CeO_2 is assigned to the presence of surface and sub-surface oxygen atoms, which are the main responsible for the improved CeO_2 oxygen storage capacity. These species are usually reduced at much lower temperature when CeO_2 is supported on a zeolite, indicating greater oxygen mobility. Fig. 5 also shows that the bulk CeO_2 presents a main reduction process at about 820 °C, which is related to the bulk reduction of the ceria with elimination of the lattice O^{2-} anions [51]. Therefore, in Fig. 5, it can be seen that the reduction peak of CeO_2 on the impregnated samples has a reduction temperature higher than 460 °C, which could mean that Ni decreases the CeO_2 oxygen mobility. Even though, the reduction temperature is not as high as for the bulk CeO_2, indicating the presence of CeO_2 small particles strongly interacting with the support [50], as already observed by XRD. Moreover, it can be observed that, with the increase of the Ce content on the catalysts, the CeO_2 reduction peak is displaced to lower temperatures. This could signify that the higher the amount of Ce, the better the oxygen storage capacity of the samples.

Thus, according to the H_2-TPR, as the reduction peak of cerium occurs at temperatures superior than the reduction pretreatment temperature (470 °C), CeO_2 should be the main cerium specie present after reduction. On the other hand, Ni should be mainly present in the reduced form (Ni^0) after the reduction pretreatment.

3.2. Catalysts activity, selectivity and stability

The performances of the several prepared catalysts were firstly evaluated by analyzing the obtained CO_2 conversions and CH_4 selectivities. It is important to refer that the only secondary product found in the reactor effluent was CO, the carbon molar balances closing at about 97–102%.

Fig. 6a compares the activity at increasing temperatures of the different catalysts containing Ni. This figure also includes the results for the pure USY zeolite, as well as the thermodynamic CO_2 equilibrium conversions at the reaction conditions (obtained with Aspen Plus®). Very low activities were observed for the 2% Ni catalyst prepared by ion-exchange, which are comparable to those found when only USY support is used. As previously observed, temperatures superior to 800 °C are required to reduce the exchanged Ni species (Fig. 3a), due to their preferential location on the hexagonal prisms, meaning that the majority of the Ni species present on this catalyst was not in the reduced form, Ni^0, during the reaction (pre-reduction at 470 °C). Therefore, the activity noticed for the ion-exchange zeolite could be mainly attributed to the USY support. This clearly shows the importance of having reduced Ni species on the catalyst to perform the reaction. Indeed, a higher activity was found for the 2% Ni catalyst prepared

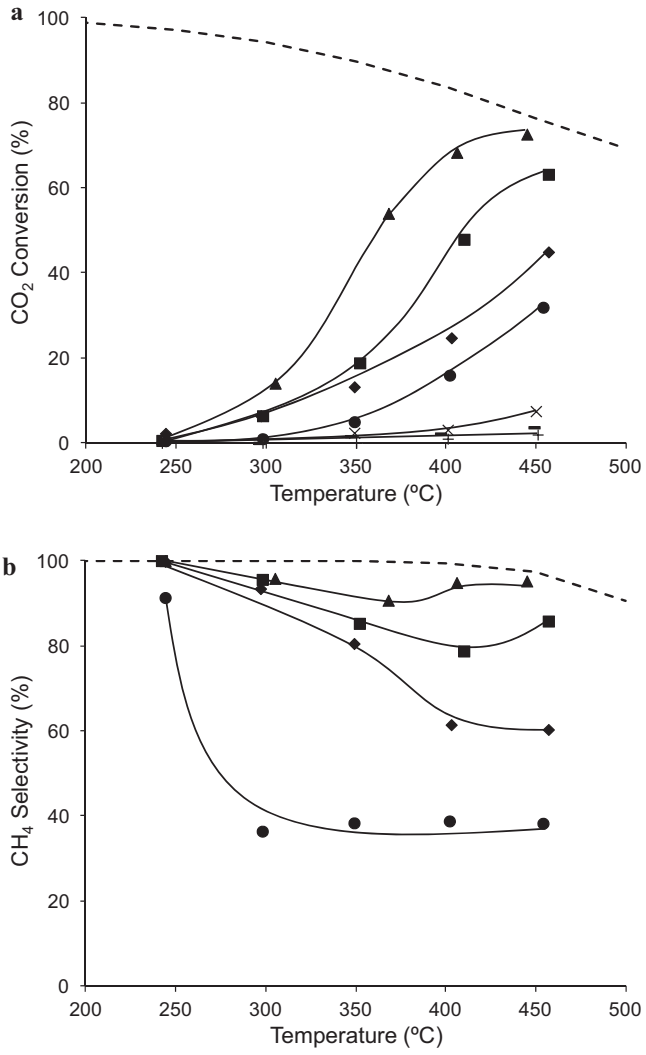

Fig. 6. (a) CO_2 conversion and (b) CH_4 selectivity vs. temperature, at GHSV = 43,000 h^{-1}, for the USY (+), 10%NiO + USY (×), 2%$NiUSY_{Ex}$ (–), 2%$NiUSY_{Imp}$ (●), 5%$NiUSY_{Imp}$ (♦), 10%$NiUSY_{Imp}$ (■) and 14%$NiUSY_{Imp}$ (▲) catalysts. Dashed line – thermodynamic equilibrium conversion values.

by impregnation, for which a greater amount of Ni species were reducible at temperatures inferior to 500 °C (Fig. 3a).

As the characterization of the highly impregnated Ni catalysts (5–14% Ni) indicated the presence of NiO as main Ni specie, before reduction, the CO_2 hydrogenation into methane was carried out over a 10%NiO + USY mechanical mixture, in order to analyze the effect of having supported Ni species, instead of unsupported. The much lower CO_2 conversions obtained for the mechanical mixture visibly indicate that an interaction between the Ni species and the support should exist, in order to attain the interesting levels of activity observed for the highly impregnated zeolites. In fact, for the impregnated samples, despite the Ni^0 particles being mainly adsorbed on the zeolite external surface, they are interacting with the zeolite support, which could explain the interesting activation levels noticed for these samples. Another parameter that usually greatly influences the catalysts activity is the size of the metal particles after reduction. Therefore, it could be supposed that the improved activity found for the impregnated zeolites might be related to the existence of smaller and better dispersed Ni particles (Fig. 7a and b) than for the mechanical mixture. This can be confirmed by the analysis of the XRD patterns of the reduced samples (Fig. 8), in which the diffraction peaks of the Ni^0 (44.5°, 51.9° and 76.3° [19]) are well visible, mainly the first one. Actually, it is possible to see that, for the mechanical mixture, the peak at 44.5° is thinner than for the impregnated zeolites, meaning that, indeed, there are larger Ni particles in the mechanical mixture. The crystallite size of the Ni particles was determined for the mechanical mixture and impregnated samples, using the Scherrer equation. The values obtained effectively revealed that the crystallite size of the Ni^0 particles in the mechanical mixture (103 nm) is much higher than for the impregnated samples (17–33 nm).

Table 3
Effect of Ce addition on the CO_2 conversion and CH_4 selectivity, at 400 °C and GHSV = 43,000 h^{-1}.

Sample	CO_2 conversion (%)	CH_4 selectivity (%)
5%$NiUSY_{Imp}$	24.7	61.4
4%Ni3%$CeUSY_{Imp}$	37.7	72.1
4%Ni7%$CeUSY_{Imp}$	44.3	75.5
5%Ni15%$CeUSY_{Imp}$	55.0	86.2
10%$NiUSY_{Imp}$	47.9	78.8
8%Ni7%$CeUSY_{Imp}$	51.7	85.6
14%$NiUSY_{Imp}$	65.5	94.2
14%Ni7%$CeUSY_{Imp}$	68.3	95.1

Furthermore, it is possible to see in Fig. 6a that, for the impregnated zeolites, there is an enhancement of the CO_2 conversion by increasing the Ni content. Indeed, for the sample with higher amount of Ni (14%), CO_2 activation occurs at lower temperatures. At 350 °C, a CO_2 conversion of 54% is already observed, being the thermodynamic equilibrium conversion almost reached at 450 °C. Likewise, an important improvement of the CH_4 selectivity was also noticed with the increase of the Ni amount from 2% to 14% (Fig. 6b). According to the H_2-TPR results (Fig. 3), these increases of the conversion and selectivity could be mainly due to the higher amount of NiO species able to be reduced at temperatures inferior to 500 °C, particularly the NiO species located on the outer surface and supercages of the zeolite.

Another interesting observation concerns the shapes of the selectivity curves (Fig. 6b). For lower amounts of Ni, there is an initial strong decrease of methane selectivity with the temperature followed by a selectivity plateau, and, for high Ni contents, a slight decrease of the methane selectivity is observed at lower temperatures and then an increase at higher temperatures. Therefore, this means that, for all the samples, there is an attenuation of the carbon monoxide formation with the increase of the temperature, which is more preponderant at higher Ni contents. Two possible explanations could be pointed out for this effect: (i) the relative preponderance of the reverse water gas shift (RWGS: $CO_2 + H_2 \leftrightarrow CO + H_2O$) reaction that leads to CO formation decreases with the temperature or (ii) at high temperatures, the formed CO is as well transformed into methane.

In order to analyze the Ce effect on the catalysts performances, samples with different Ce contents were prepared by impregnation of the Ni catalysts. Fig. 9 shows the evolution of the CO_2 conversion and CH_4 selectivity with temperature for catalysts containing different Ce contents, all prepared from the 5%Ni zeolite. The addition of Ce is responsible for a gradual improvement of both CO_2 conversion and CH_4 selectivity with the increase of Ce content, as observed by other authors [23–25], which could be related with the higher oxygen storage capacity found for these samples with the increase of Ce amount (Fig. 5). This positive effect of Ce is as well visible for samples presenting higher amounts of Ni (10 and 14%, Fig. 10). Table 3 clearly shows the improvement of catalysts performances resulting from Ce incorporation. Indeed, for the group of zeolite samples prepared from the 5%NiUSY sample, increases in the CO_2 conversion and CH_4 selectivity of about 123 and 40% were, respectively, noticed, at 400 °C. For the catalysts with higher Ni contents,

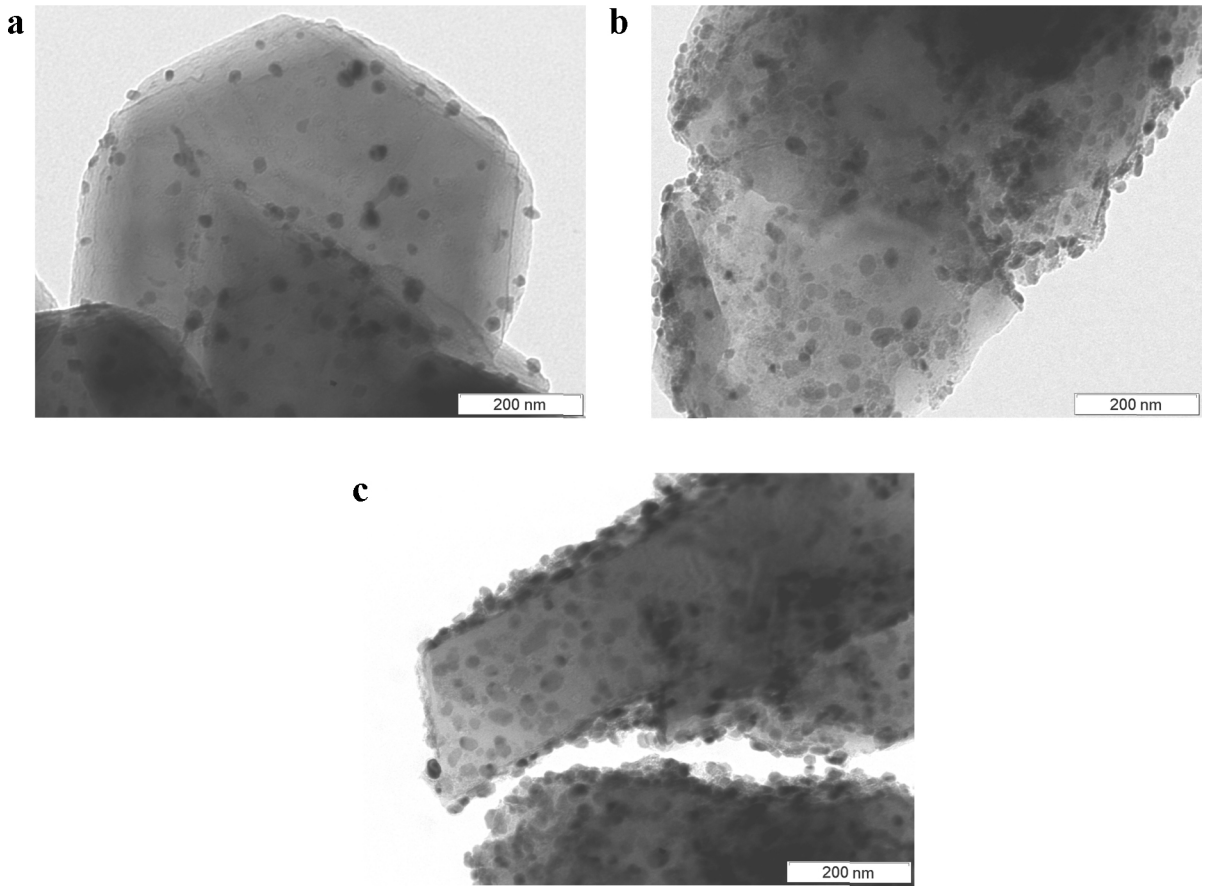

Fig. 7. TEM micrographs for the (a) 5%NiUSY$_{Imp}$ and (b) 14%NiUSY$_{Imp}$ after reduction, and for the (c) 14%NiUSY$_{Imp}$ after 10 h of reaction at 400 °C.

enhancements of both CO_2 conversion and CH_4 selectivity are also observed in presence of Ce, but these are less pronounced (1–9%), mainly for the 14%Ni catalysts, due to the higher proximity to the equilibrium values at 400 °C.

Based on the UV–vis spectroscopy and H_2-TPR data, it was possible to confirm that, after reduction, Ce is mainly present as CeO_2. These Ce species have been claimed in the literature as able to activate CO_2 molecules and reduce them into CO due to the great mobility of the oxygen atoms [18–26]. The O mobility within the non-stoichiometric cerium oxide is related to oxygen vacancies formation that can promote the CO_2 adsorption and its transformation into CO, which can be subsequently hydrogenated into methane. With the purpose to verify this hypothesis, a catalyst impregnated only with 7% of Ce containing CeO_2 was tested (Fig. 9a and b). Despite the very low conversions obtained (about 2% at 450 °C), an interesting result was the poor methane selectivities, inferior to 50%, found with this catalyst, which could indicate that CeO_2 present on the catalyst mainly promotes the CO_2 transformation into CO. In fact, an effect of the support (USY zeolite) for the low CH_4 selectivities observed with the 7%CeUSY catalysts can be excluded, since, for the USY zeolite, at the same conversion levels, the obtained CH_4 selectivities were not inferior to 76%. Therefore, the Ce addition should lead to a preferential formation of CO. Nevertheless, it should be also important to consider the probable existence of synergetic effects between the metal active sites and the promoter, including a possible nickel dispersion improvement due to the presence of Ce, as important factors in the final catalyst properties.

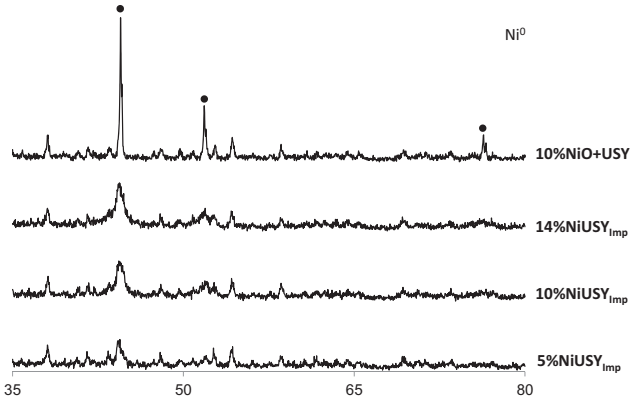

Fig. 8. X-ray diffractograms for the mechanical mixture and impregnated catalysts, after reduction.

To reach conclusions about the zeolite-based catalysts interest to perform the CO_2 methanation reaction, it is important to compare the performances of the most active and selective zeolite-based catalysts with those obtained for the catalysts found in the literature (Table 4) [18–20,52–56]. However, the operating conditions used in the studies are very different, so that this comparison will be focused on the catalysts tested under operating conditions similar to those used in the present work, i.e. the 15%Ni/RHA-Al_2O_3, the 5%Ni-$Ce_{0.5}Zr_{0.5}O_2$ and the 10%Ni-$Ce_{0.72}Zr_{0.28}O_2$. For the two later catalysts, it is possible to observe that, even if the contact times used in the present study are lower (in some cases four times

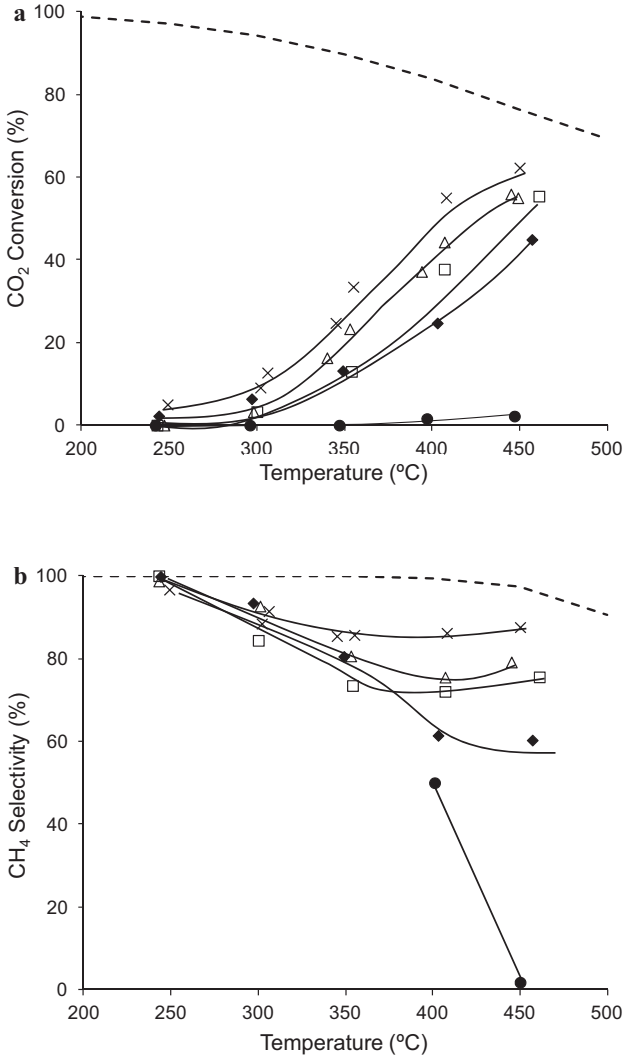

Fig. 9. (a) CO_2 conversion and (b) CH_4 selectivity vs. temperature, at GHSV = 43,000 h^{-1}, for the 7%CeUSY$_{Imp}$ (●), 5%NiUSY$_{Imp}$ (♦), 4%Ni3%CeUSY$_{Imp}$ (□), 4%Ni7%CeUSY$_{Imp}$ (△) and 5%Ni15%CeUSY$_{Imp}$ (×) catalysts. Dashed line – thermodynamic equilibrium conversion values.

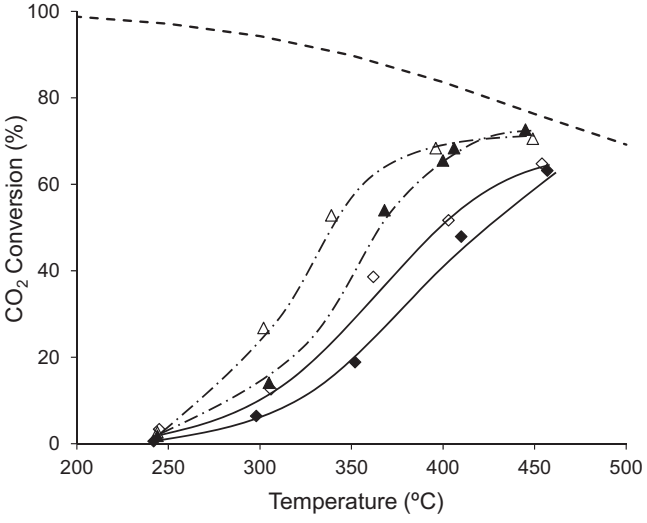

Fig. 10. (a) CO_2 conversion vs. temperature, at GHSV = 43,000 h^{-1}, for the 10%NiUSY$_{Imp}$ (♦), 8%Ni7%CeUSY$_{Imp}$ (◊), 14%NiUSY$_{Imp}$ (▲) and 14%Ni7%CeUSY$_{Imp}$ (△) catalysts. Dashed line – thermodynamic equilibrium conversion values.

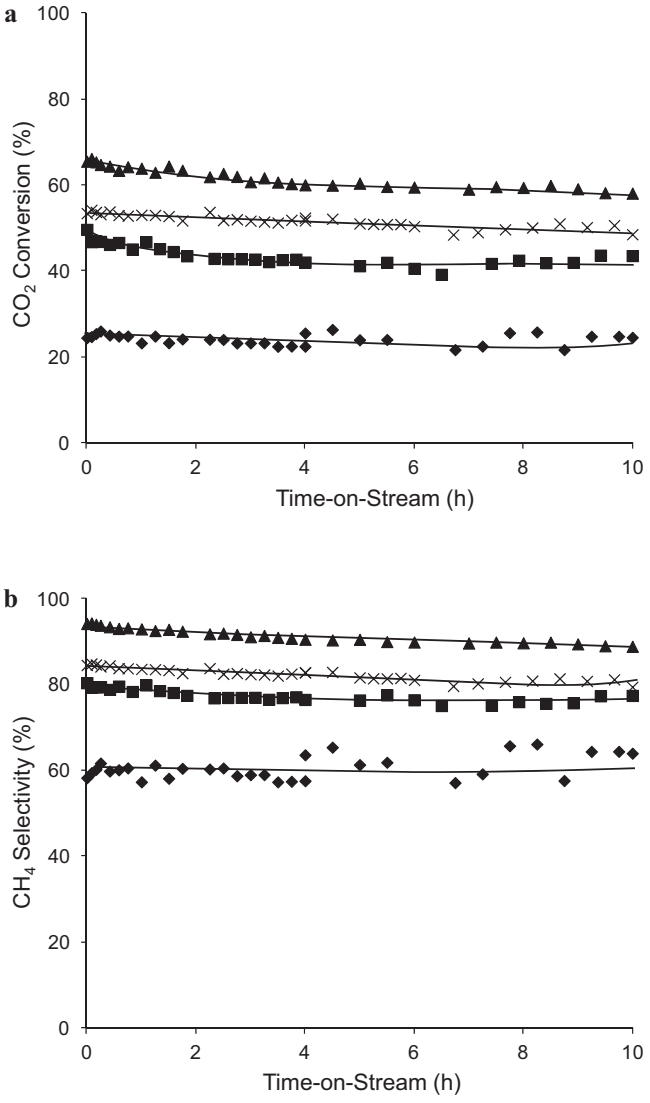

Fig. 11. Evolution of the (a) CO_2 conversion and (b) CH_4 selectivity with the time-on-stream, at GHSV = 43,000 h^{-1}, for the 5%NiUSY$_{Imp}$ (♦), 10%NiUSY$_{Imp}$ (■), 14%NiUSY$_{Imp}$ (▲) and 5%Ni15%CeUSY$_{Imp}$ (×) catalysts.

smaller), the results are not significantly different. Furthermore, it can be seen that, for the zeolite-based catalysts, when the contact time increases, the CO_2 conversion, CH_4 selectivity and CH_4 yield become very similar to the values obtained for the Ce–Zr mixed oxides, even though the contact time is not as high as for the Ce–Zr mixed oxides. Comparing the results obtained for the zeolite-based catalysts for a contact time of 1.4 min with those presented in Table 4 for the 15%Ni/RHA-Al_2O_3 catalyst, it can be observed that the former catalyst present better CO_2 conversions, CH_4 selectivities and CH_4 yields, at a lower temperature.

Finally, the stability of the catalysts after 10 h of reaction at 400 °C was evaluated. In general, all the Ni and Ce supported zeolites, even those containing high amounts of metals, revealed somewhat stable, in terms of CO_2 conversion and CH_4 selectivity (Fig. 11). The deactivation only slightly increases with the increase of metals content. In fact, no significant changes of the Ni particles size were observed by TEM after 10 h of reaction (Fig. 7b and c).

Therefore, it is possible to conclude that our preliminary results show that zeolites are interesting supports for the CO_2 hydrogenation into methane.

Table 4
Comparison between the results obtained for the most performing zeolite-based catalysts and those found in the literature for other catalysts [18–20,52–56].

Sample	T (°C)	P_{CO_2} (atm)	H_2:CO_2	GHSV (h^{-1})	Contact time[a] (min)	$Flux_{tot}/m_{cat}$ (mL s^{-1} g^{-1})	CO_2 conversion (%)	CH_4 selectivity (%)	CH_4 yield (%)
$Ce_{0.95}Ru_{0.05}O_2$	450	0.13	4	61,000	0.8	12.5	55	99	~55
3%Ni-MCM-41	400	0.28	2.6	–	8.0	1.6	17	96	16
6.2%Pd-3.6%Mg/SiO_2	450	0.17	4	–	5.2	2.0	59	95	56
6.2%Pd-3.6%Ni/SiO_2	450	0.17	4	–	5.2	2.0	50	89	45
12%Ni/ZrO_2-Al_2O_3	360	0.22	3.5	–	5.6	2.3	73	97	71
5%Ni/$La_2O_2CO_3$	300	0.20	4	–	6.1	2.1	40	89	36
15%Ni/RHA-Al_2O_3	500	0.20	4	–	1.5	8.3	64	91	58
5%Ni-$Ce_{0.5}Zr_{0.5}O_2$	400	0.16	4	43,000	2.0	6.1	80	~99	79
10%Ni-$Ce_{0.72}Zr_{0.28}O_2$	400	0.16	4	43,000	2.0	6.1	85	~99	84
14%$NiUSY_{Imp}$	400	0.16	4	43,000	0.5	23.9	65.5	94.2	61.7
14%Ni7%$CeUSY_{Imp}$	400	0.16	4	43,000	0.5	23.9	68.3	95.1	65.0
14%$NiUSY_{Imp}$	400	0.16	4	15,000	1.4	8.3	74.8	98.5	73.7
14%Ni7%$CeUSY_{Imp}$	400	0.16	4	15,000	1.4	8.3	77.1	99.1	76.4

[a] Taken as the reverse of the weight hourly space velocity (WHSV).

4. Conclusion

Catalysts containing Ni and Ce supported on a HNaUSY zeolite were tested for the CO_2 hydrogenation into methane. The results pointed out that, when prepared by impregnation, Ni-zeolite catalysts present very interesting levels of activity and selectivity for this reaction because of the easier reducibility of the NiO species, compared to the ion-exchanged Ni species. In fact, it was observed that the higher the Ni content on the catalysts, the better their performances, due to the greater amount of Ni^0 species after reduction. The Ce addition to the Ni zeolites is also responsible for a further improvement of the catalysts activity and selectivity, which could be attributed to the presence of CeO_2 that promotes the CO_2 conversion into CO. Therefore, the final catalyst properties result from a synergetic effect between the metal active sites and the promoter. Furthermore, all these catalysts revealed a good stability when submitted to 10 h of reaction at 400 °C, with no sintering occurring.

Hence, this work shows that Ni-zeolites could be used to perform the CO_2 hydrogenation reaction into methane, being the conversions and selectivities obtained comparable to those found for the best CO_2 methanation catalysts reported in the literature that use potentially more expensive bulk cerium oxide supports. Additionally, a wide window of future research possibilities is opened since the well known zeolite properties can be easily modulated, inducing relevant changes in the properties of the adsorbed metals. Further work is already currently being accomplished, in order to optimize this type of catalysts.

Acknowledgment

I. Graça thanks the Fundação para a Ciência e a Tecnologia (FCT) for her Post-Doc. grant (SFRH/BPD/74457/2010).

References

[1] CO_2 Emissions from Fuel Combustion – Highlights, 2009 Edition, IEA – Statistics, International Energy Agency, 2009.
[2] World Energy Outlook 2008, International Energy Agency, 2008.
[3] C. Song, Catal. Today 115 (2006) 2–32.
[4] G. Aydin, I. Karakurt, K. Aydiner, Energy Policy 38 (2010) 5072–5080.
[5] G. Centi, S. Perathoner, Catal. Today 148 (2009) 191–205.
[6] J. Ma, N. Sun, X. Zhang, N. Zhao, F. Xiao, W. Wei, Y. Sun, Catal. Today 148 (2009) 221–231.
[7] X. Xiaoding, J.A. Moulijn, Energy Fuels 10 (1996) 305–325.
[8] K.M.K. Yu, I. Curcic, J. Gabriel, S.C.E. Tsang, ChemSusChem 1 (2008) 893–899.
[9] T. Inui, T. Takeguchi, Catal. Today 10 (1991) 95–106.
[10] K. Hashimoto, H. Habazaki, M. Yamasaki, S. Meguro, T. Sasaki, H. Katagiri, T. Matsui, K. Fujimura, K. Izumiya, N. Kumagai, E. Akiyama, Mater. Sci. Eng. 304–306 (2001) 88–96.
[11] W. Wang, J. Gong, Front. Chem. Sci. Eng. 5 (2011) 2–10.
[12] E. Zagli, J. Falconer, J. Catal. 62 (1980) 280–285.
[13] E. Zagli, J. Falconer, J. Catal. 69 (1981) 1–8.
[14] G.D. Weatherbee, C.H. Bartholomew, J. Catal. 87 (1984) 352–362.
[15] P. Panagiotopoulou, D.I. Kondarides, X.E. Verykios, Appl. Catal. A: Gen. 344 (2008) 45–54.
[16] M. Agnelli, M. Kolb, C. Nicot, C. Mirodatos, Stud. Surf. Sci. Catal. 68 (1991) 605–612.
[17] M. Agnelli, M. Kolb, C. Mirodatos, J. Catal. 148 (1994) 9–21.
[18] F. Ocampo, B. Louis, A.C. Roger, Appl. Catal. A: Gen. 392 (2011) 36–44.
[19] F. Ocampo, B. Louis, A.C. Roger, Appl. Catal. A: Gen. 369 (2009) 90–96.
[20] S. Sharma, Z. Hu, P. Zhang, E.W. McFarland, H. Metiu, J. Catal. 278 (2011) 297–309.
[21] S. Tada, T. Shimizu, H. Kameyama, T. Haneda, R. Kikuchi, Int. J. Hydrogen Energy 37 (2012) 5527–5531.
[22] A. Trovarelli, C. de Leitenburg, G. Dolcetti, J. Chem. Soc. Chem. Commun. (1991) 472–473.
[23] A. Trovarelli, C. de Leitenburg, G. Dolcetti, J. Llorca, J. Catal. 151 (1995) 111–124.
[24] K.O. Xavier, R. Streekala, K.K.A. Rashid, K.K.M. Yusuff, B. Sen, Catal. Today 49 (1999) 17–21.
[25] J.M. Rynkowski, T. Paryjczak, A. Lewicki, M.I. Szynkowska, T.P. Maniecki, W.K. Jóźwiak, React. Kinet. Catal. Lett. 71 (2000) 55–64.
[26] C. de Leitenburg, A. Trovarelli, J. Kašpar, J. Catal. 166 (1997) 98–107.
[27] D.J. Elliot, J.H. Lunsford, J. Catal. 57 (1979) 11–26.
[28] N.C. Saha, E.E. Wolf, Appl. Catal. 13 (1984) 101–112.
[29] S. Scirè, C. Crisafulli, R. Maggiore, S. Minicò, S. Galvagno, Catal. Lett. 51 (1998) 41–45.
[30] S. Eckle, H.-G. Anfang, R.J. Behm, J. Phys. Chem. C 115 (2011) 1361–1367.
[31] V. Patzelová, A. Zukal, Z. Tvarůžkova, O. Malíček, Stud. Surf. Sci. Catal. 18 (1984) 367–374.
[32] D.W. Breck, E.M. Flamigen, Molecular Sieves, Society of Chemical Industry, London, 1968.
[33] S.J. Gregg, K.S.W. Sing, Adsorption Surface Area and Porosity, 2nd ed., Academic Press, London, 1982.
[34] G. Leofanti, M. Padovan, G. Tozzola, B. Venturelli, Catal. Today 41 (1998) 207–219.
[35] Á. Kukovecz, Z. Kónya, D. Mönter, W. Reschetilowski, I. Kiricsi, J. Mol. Struct. 563–564 (2001) 403–407.
[36] L. Espinosa-Alonso, K.P. Jong, B.M. Weckhuysen, J. Phys. Chem. C 112 (2008) 7201–7209.
[37] R. Baran, I.I. Kamińska, A. Śrębowata, S. Dzwigaj, Microporous Mesoporous Mater. 169 (2013) 120–127.
[38] Y. Qi, H. Qi, J. Li, C. Lu, J. Cryst. Growth 310 (2008) 4221–4225.
[39] M. Suzuki, K. Tsutsumi, H. Takahashi, Y. Saito, Zeolites 9 (1989) 98–102.
[40] D.H. Olson, J. Phys. Chem. 72 (1968) 4366–4373.
[41] L. Daza, B. Pawelec, J.A. Anderson, J.L.G. Fierro, Appl. Catal. A: Gen. 87 (1992) 145–156.
[42] B. Pawelec, R. Mariscal, R.M. Navarro, J.M. Campos-Martin, J.L.G. Fierro, Appl. Catal. A: Gen. 262 (2004) 155–166.
[43] A. Luengnaruemitchai, A. Kaengsilalai, Chem. Eng. J. 144 (2008) 96–102.
[44] E. Sahle-Demessie, V.G. Devulapelli, A.A. Hassan, Catalysts 2 (2012) 85–100.
[45] L.F. Córdoba, M. Flytzani-Stephanopoulos, C.M. de Correa, Appl. Catal. B: Environ. 33 (2001) 25–33.
[46] S. Damyanova, C.A. Perez, M. Schmal, J.M.C Bueno, Characterization of ceria-coated alumina carrier, Appl. Catal. A: Gen. 234 (2002) 271–282.
[47] J.K. Reddy, G. Suresh, C.H. Hymavathi, V.D. Kumari, M. Subrahmanyam, Catal. Today 141 (2009) 89–93.
[48] F.A.C. Garcia, D.R. Araújo, J.C.M. Silva, J.L. de Macedo, G.F. Ghesti, S.C.L. Dias, G.N.R. Filho, J. Braz. Chem. Soc. 22 (2011) 1894–1902.

[49] C.R. Moreira, M.M. Pereira, X. Alcobé, N. Homs, J. Llorca, J.L.G. Fierro, P.R. de la Piscina, Microporous Mesoporous Mater. 100 (2007) 276–286.
[50] Q. Huang, X. Xue, R. Zhou, J. Mol. Catal. A: Chem. 331 (2010) 130–136.
[51] C. Bigey, L. Hilaire, G. Maire, J. Catal. 198 (2001) 208–222.
[52] G.A. Du, S. Lim, Y.H. Yang, C. Wang, L. Pfefferle, G.L. Haller, J. Catal. 249 (2007) 370–379.
[53] J.N. Park, E.W. McFarland, J. Catal. 266 (2009) 92–97.
[54] M. Cai, J. Wen, W. Chu, X. Cheng, Z. Li, J. Nat. Gas Chem. 20 (2011) 318–324.
[55] J. Gao, L.S. Jia, W.P. Fang, Q.B. Li, H. Song, J. Fuel Chem. Technol. 37 (2009) 573–577.
[56] F.W. Chang, M.S. Kuo, M.T. Tsay, M.C. Hsieh, Appl. Catal. A 247 (2003) 309–320.